Depolarization composition of backscattered circularly polarized light

Ivan Lopushenko and Alexander Bykov

Opto-Electronics and Measurement Techniques, ITEE, University of Oulu, Oulu 90014, Finland

Igor Meglinski[*]

College of Engineering and Physical Sciences, Aston University, Birmingham B4 7ET, United Kingdom

We consider the origin of unpolarized light resulting from the backscattering of circularly polarized light by a random turbid tissuelike disperse medium. We reveal the dynamics of the backscattered fraction of unpolarized light, disclosing its meticulous decomposition into two rigorously polarized components characterized by opposing helicities, with fully defined polarization states. Concurrently, their superposition, driven by multiple scattering within the medium, leads to the appearance of a fraction of linear polarization. We emphasize that the in-depth binding of circular polarization memory of light when the helicity flips occurs within the scattering medium, meaning the conservation of spin angular momentum. We anticipate that the results obtained hold significant implications for future studies, particularly in the field of tissue polarimetry and light vortices.

In conjunction with the wavelength and coherence, polarization is a fundamental property of light [1] attracting great attention in numerous practical biomedical and clinical applications [2–4]. Circularly polarized light carries an intrinsic angular momentum due to its polarization helicity [5]. Recent studies have shown that the phase retardation of circularly polarized light, backscattered by biological tissue, can be used effectively for the quantitative evaluation of cervical intraepithelial neoplasia [6], the presence of senile Alzheimer's plaques [7,8], and the characterization of biological tissues with optical anisotropy [9,10]. This polarimetry approach is based on the directional awareness of circularly polarized light, where, by the known stage of polarization of incident light, the helicity of scattered light can be used to determine if it has been forward scattered or backscattered [11]. This peculiar property of circularly polarized light is also known as polarization memory [12,13]. The directional awareness of circularly polarized light is a manifestation of the anisotropy of scattering [14]. Linear polarization possesses no such sense of directional awareness. Scattered multiple numbers of times in a turbid tissuelike disordered medium, linearly or circularly polarized light is depolarized, and the depolarization degree depends strongly on the size and shape of the scattering particles [15,16], as well as on the number of scattering events [17]. Quantitatively, the residual state of polarization is defined as the ratio of polarized intensity to the total intensity of backscattered light, known as a degree of polarization (DP).

DP is defined utilizing Stokes vector parameters [1] as

$$P = \frac{\sqrt{S_1^2 + S_2^2 + S_3^2}}{S_0}. \tag{1}$$

Here, S_1 is the difference in intensity between horizontally and vertically polarized light ($S_1 = I_\parallel - I_\perp$), S_2 is the difference in intensity between linearly polarized light observed at $45°$ and $-45°$ ($S_2 = I_{+45°} - I_{-45°}$), S_3 is the difference in intensity between left- and right-circularly polarized light ($S_3 = I_L - I_R$), and S_0 is the total intensity of light ($S_0 = I_\parallel + I_\perp = I_{+45°} + I_{-45°} = I_L + I_R$).

The circularly polarized light backscattered from a turbid tissuelike disordered medium is represented as a sum of two Stokes vectors defining unpolarized and totally polarized light [1]:

$$\begin{pmatrix} S_0 \\ S_1 \\ S_2 \\ S_3 \end{pmatrix} = (1-P) \begin{pmatrix} S_0 \\ 0 \\ 0 \\ 0 \end{pmatrix} + \begin{pmatrix} PS_0 \\ S_1 \\ S_2 \\ S_3 \end{pmatrix}, \quad 0 \leqslant P \leqslant 1. \tag{2}$$

In addition to the overall P, there are specific measures of the degree for different types of polarization:

$$P_L = \frac{\sqrt{S_1^2 + S_2^2}}{S_0}, \tag{3}$$

and

$$P_C = \frac{\sqrt{S_3^2}}{S_0}. \tag{4}$$

Here, P_L and P_C are, respectively, the degree of linear polarization (DLP) and the degree of circular polarization (DCP)

*Correspondening author: i.meglinski@aston.ac.uk

$(P^2 = P_L^2 + P_C^2)$. In practice, P_C is often presented as [18]

$$P_C = \frac{S_3}{S_0} = \frac{I_L - I_R}{I_L + I_R}, \qquad (5)$$

also known as circular intensity differential scattering (CIDS) [19], showing the degree of differential scattering between measured intensities of left and right circular polarization, and providing a quantitative measure of polarization-preserving properties of the scattering medium.

Partially polarized light is decomposed into two completely polarized fractions of light with opposite helicity [1]:

$$\begin{pmatrix} S_0 \\ S_1 \\ S_2 \\ S_3 \end{pmatrix} = \frac{(1+P)}{2P} \begin{pmatrix} PS_0 \\ S_1 \\ S_2 \\ S_3 \end{pmatrix} + \frac{(1-P)}{2P} \begin{pmatrix} PS_0 \\ -S_1 \\ -S_2 \\ -S_3 \end{pmatrix}. \qquad (6)$$

From a practical point of view, expression (2) is represented in terms of Stokes parameters normalized to the intensity of the fully polarized component, i.e.,

$$Q = \frac{S_1}{PS_0}, \quad U = \frac{S_2}{PS_0}, \quad V = \frac{S_3}{PS_0}. \qquad (7)$$

This allows us to assess quantitatively the parameters of the Stokes vector observed by a conventional polarimeter [20]. Thus, for light depolarized due to propagation through a turbid tissuelike scattering medium, (2) takes the form

$$\begin{pmatrix} S_0 \\ S_1 \\ S_2 \\ S_3 \end{pmatrix} = (1-P)S_0 \begin{pmatrix} 1 \\ 0 \\ 0 \\ 0 \end{pmatrix} + PS_0 \begin{pmatrix} 1 \\ Q \\ U \\ V \end{pmatrix}. \qquad (8)$$

In a turbid scattering medium, such as biological tissue, the P drop can be significant, leading to a significant decrease of the signal-to-noise ratio and a loss of sensitivity and accuracy in optical measurements [4].

By analogy to (6), partially depolarized ($0 < P_C < 1$) backscattered circularly polarized light is presented in terms of a specific polarization measure (4) as a sum of totally polarized and completely unpolarized light that according to (8) can be also decomposed into two opposite polarization states:

$$\begin{pmatrix} S_0 \\ 0 \\ 0 \\ S_3 \end{pmatrix} = P_C S_0 \begin{pmatrix} 1 \\ 0 \\ 0 \\ 1 \end{pmatrix} + (1-P_C) \left[\frac{S_0}{2} \begin{pmatrix} 1 \\ 0 \\ 0 \\ -1 \end{pmatrix} + \frac{S_0}{2} \begin{pmatrix} 1 \\ 0 \\ 0 \\ 1 \end{pmatrix} \right]. \qquad (9)$$

Thus, backscattered from the medium, circularly polarized light can be represented as a decomposition of two totally polarized left-circularly polarized (LCP) and right-circularly polarized (RCP) components:

$$\begin{pmatrix} S_0 \\ 0 \\ 0 \\ S_3 \end{pmatrix} = \frac{(1-P_C)S_0}{2} \begin{pmatrix} 1 \\ 0 \\ 0 \\ -1 \end{pmatrix} + \frac{(1+P_C)S_0}{2} \begin{pmatrix} 1 \\ 0 \\ 0 \\ 1 \end{pmatrix}. \qquad (10)$$

In a similar way the depolarized linearly polarized light can be also presented as a decomposition of linear horizontal $I_{\parallel}$ and vertical $I_{\perp}$ states of polarization,

$$\begin{pmatrix} S_0 \\ S_1 \\ S_2 \\ 0 \end{pmatrix} = \frac{(1+P_L)S_0}{2} \begin{pmatrix} 1 \\ Q \\ U \\ 0 \end{pmatrix} + \frac{(1-P_L)S_0}{2} \begin{pmatrix} 1 \\ -Q \\ -U \\ 0 \end{pmatrix}, \qquad (11)$$

that reduce accordingly to

$$\begin{pmatrix} S_0 \\ S_1 \\ 0 \\ 0 \end{pmatrix} = \frac{(1+\delta_R)S_0}{2} \begin{pmatrix} 1 \\ 1 \\ 0 \\ 0 \end{pmatrix} + \frac{(1-\delta_R)S_0}{2} \begin{pmatrix} 1 \\ -1 \\ 0 \\ 0 \end{pmatrix}, \qquad (12)$$

if $S_2 = 0$. Here,

$$\delta_R = \sqrt{S_1^2}/S_0 = \frac{I_{\parallel} - I_{\perp}}{I_{\parallel} + I_{\perp}} \qquad (13)$$

is the depolarization ratio [17] for linearly polarized light, defined as the ratio of the intensity of polarized light to the total intensity.

The experimental approach commonly employed for direct measurements of the intensity of the backscattered polarized light, as well as P, P_L, P_C, δ_R quantities [6–8,11,21,22], is

depicted schematically in Fig. 1. The transformation of low-coherent laser light into RCP, achieved using a set of lenses, and half-wave and quarter-wave plates, facilitates its focused delivery onto the turbid tissuelike scattering medium or tissue sample. The photons entering into the medium undergo a sequence of scattering events before they are detected. Backscattered light is collected by an objective positioned at a particular distance ρ from the point of incidence and subsequently passed through an analyzer to measure its polarization state. The trajectories of photons within the medium,
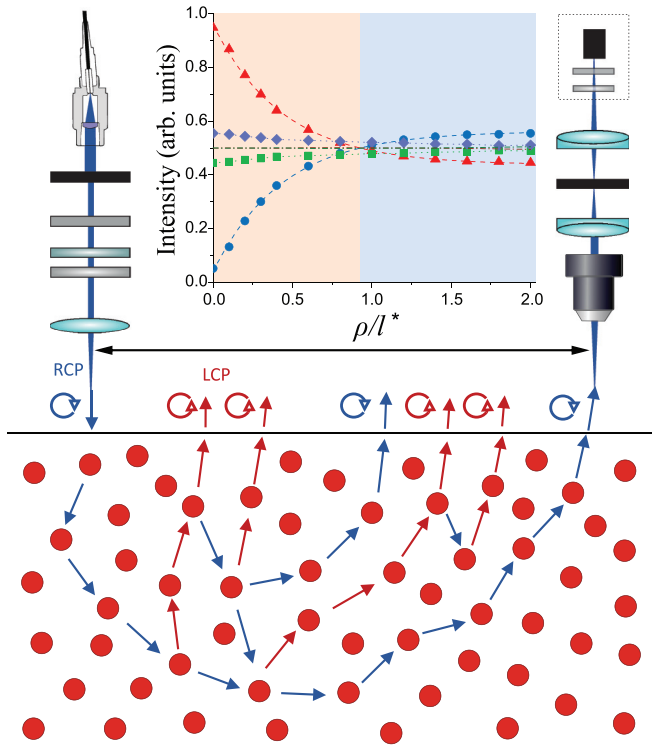
FIG. 1. Schematic presentation of the experimental setup, along with selected potential photon trajectories within the medium, wherein each backscattering event induces a helicity flip, visually depicted by the color of the directional arrow. The inset shows LCP (▲) and RCP (●) components of the backscattered RCP light, and the pairs of orthogonal intensities $I_\parallel$ (■), $I_\perp$ (◇) and $I_{+45°}$ (black line), $I_{-45°}$ (dark green line), depending on the scaled source-detector separation ρ/l^*.

schematically shown in Fig. 1, are determined by a random walk characterized by a mean free path l, ultimately culminating in their exit point, where the measured state of polarization is determined.

In this study, we consider the placement of the light source and detector to be perpendicular to the surface of the semi-infinite homogeneous turbid tissuelike scattering medium. The following parameters of the medium are used both in experiment and theoretical modeling: scattering coefficient $\mu_s = 4$ mm^{-1} ($\mu_s = 1/l$), absorption coefficient $\mu_a = 0.05$ mm^{-1}, anisotropy scattering factor $g = 0.9$, refractive index $n = 1.46$ at the wavelength of incident light $\lambda = 640$ nm ($l \gg \lambda$); $g \equiv \langle \cos \theta \rangle$, where θ is the scattering angle and the average $\langle \cdots \rangle$ is taken over the form factor of the medium scattering particle. In our experimental investigations, phantoms possessing the aforementioned optical properties are meticulously designed and crafted in accordance with established manufacturing protocols [23,24].

Figure 1 also illustrates the interplay between the oppositely polarized components of the detected light. The ρ is scaled to the transport mean free path [$l^* = 1/(1 - g)$], the average distance that light propagates before its direction of propagation is totally randomized [25].

As is evident in the inset of Fig. 1, for short source-detector separations ($\rho/l^* < 1$), the helicity of the incident RCP light

undergoes flipping as a result of backscattering. The flipped LCP light is inversely related to the emerging RCP component (see Fig. 1). The LCP light is formed due to the odd number of helicity flips occurring along the consecutive scattering events within the medium between the points of incidence and detection, whereas the appearance of RCP is based on an even number of flips [12]. The decrease of LCP with an increase of source-detector separation is compensated with a proportional increase of RCP light (see Fig. 1), clearly illustrating predictions (10). The RCP stream becomes dominating over LCP at a larger source-detector separation ($\rho > l^*$), meaning that the conservation of angular momentum is preserved, and multiple scattering maintains the helicity of incident circularly polarized light, i.e., RCP. At the isosbestic point (see Fig. 1) the intensities of two streams of light with opposite helicities are equalized ($I_L = I_R$) and linear polarization originates from their superposition. The orthogonal linearly polarized components $I_\parallel$, $I_\perp$ and $I_{+45°}$, $I_{-45°}$, engendered due to the scattering of incident RCP light by means of a superposition of the fully polarized, flipped, LCP light, and the appearance with an RCP component of opposite helicity, are also presented in Fig. 1.

Polarization memory is revealed as a flip of the backscattered circularly polarized light at the source-detector separation over the transport length ($\rho > l^*$), tailing the helicity of incident RCP light (see Fig. 1).

The results presented in Fig. 1 and figures below are attained using a Monte Carlo (MC) modeling approach grounded in the iterative procedure of the solution of the Bethe-Salpeter (BS) equation [26]. The merits of this MC methodology affirm a direct correspondence with the analytic Milne solution [27] and an inherently comprehensible physical elucidation of the coherent effects of multiple scattering of light through the utilization of ladder diagrams [26]. By employing the Jones vector formalism, this numerical scheme has been established as efficacious for tracking the polarization of photons within a turbid tissuelike medium and for simulating coherent backscattering phenomena [28]. The validity of the approach has been justified on a fundamental level [29].

A comparison of P, P_L, and P_C with the scaled source-detector separation ρ/l^* is presented in Fig. 2. P_C represents the fraction of the circularly polarized light that is preserved or retained after multiple scattering. With an increase of source-detector separation the P_C is decreased due to a reduction of the low scattering order contribution to the backscattered light. At a particular source-detector separation (ρ/l^*) where the flipped I_L and preserved I_R components of the backscattered circularly polarized light are equalized (see Fig. 2), the P_C reaches a minimum value. The minimum of P_L is observed at the same point due to parities of pairs $I_\parallel$, $I_\perp$ and $I_{+45°}$, $I_{-45°}$ (see Fig. 1). As a result, P reaches a minimal value at the same distance as well (see Fig. 2). The depolarization minimum represents the point at which the components of scattered circularly light with opposite helicity, LCP and RCP, are superimposed. The depolarization minimum coincides with the demarcation line between nondiffusive and diffusing path lengths of scattering photons characterized by l^* (see Fig. 2). These results are in a good agreement with the results of experimental studies performed earlier [8], as shown in Fig. 2. The inset presented in Fig. 2 shows the ratio of circular to
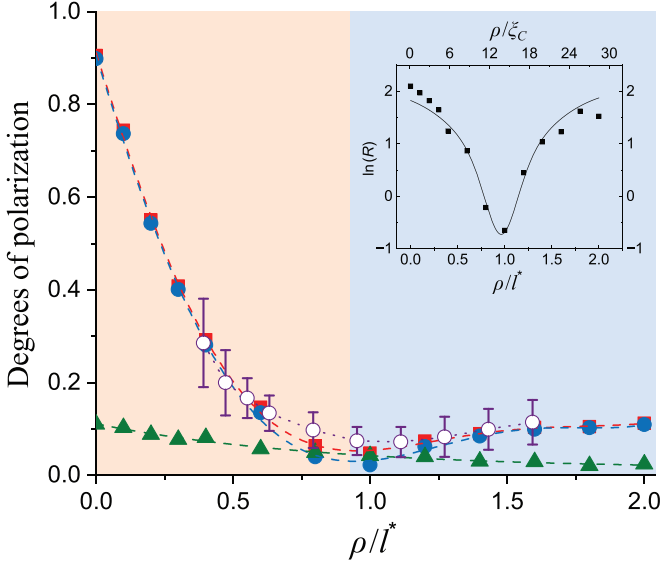
FIG. 2. P (■), P_C (●), and P_L (▲) plotted as a function of scaled source-detector separation ρ/l^*. The purple line (○) corresponds to the experimental data. The inset depicts the ratio of circular to linear degree of polarization $R = P_C/P_L$ as a function of ρ/l^* (bottom) and/or by source-detector separation scaled by a characteristic depolarization length (ρ/ξ_C) for the circularly polarized light (top).

linear degrees of polarization $R = P_C/P_L$ as a function of ρ/l^* and the source-detector separation scaled by characteristic depolarization lengths for circularly polarized light ξ_C [15,30]. This so-called circular depolarization ratio (CDR) [31] specifically quantifies the balance between circularly polarized and linearly polarized components of light within the multiple scattering. The results in the inset show that the portion of the backscattered light that retains its circular polarization versus the portion that becomes linearly polarized is dropped down quickly and reversely raised upon the helicity flip (see Fig. 2).

The extent of polarization cross-talk between the flipped and preserved components of the backscattered circularly polarized light is characterized by the polarization extinction ratio (PER) [32] ($\mathcal{E} = I_L/I_R$). Figure 3 shows the in-depth spatial distribution of the polarization memory, presented by analogy to the photon-measurement density function (PMDF) [33], in terms of the gradient of PER [$\nabla\mathcal{E}_{\mathrm{LCP/RCP}}(\mathbf{r}) = \partial\mathcal{E}/\partial x, \partial\mathcal{E}/\partial y, \partial\mathcal{E}/\partial z$] at each pixel [$\mathbf{r} = (x, y, z)$] in the medium:

$$\mathcal{E}_{\mathrm{LCP/RCP}}(\mathbf{r}) = \frac{\sum_{i=1}^{N_{\mathrm{ph}}} s_i(\mathbf{r})I_{L|R}}{s_0 \sum_{i=1}^{N_{\mathrm{ph}}} I_{L|R}}. \tag{14}$$

Here, $I_{L|R}$ corresponds to the detected LCP and/or LCP intensities, $s_i(\mathbf{r})$ is the path length of the ith photon within a pixel centered at $\mathbf{r}$, s_0 is the linear size of the pixel, and N_{ph} is the total number of detected photons. The in-depth spatial distribution (see Fig. 3) shows a strong localization of the LCP component in relation to the incident polarization state at short ($\rho < l^*$) source-detector distances. The linear polarization, emerging as a superposition of LCP and RCP components, demarcates areas of their localization. The wide aperture of the light source [numerical aperture (NA) $\sim 70°$] and anisotropy of scattering (g) result in a broad range of
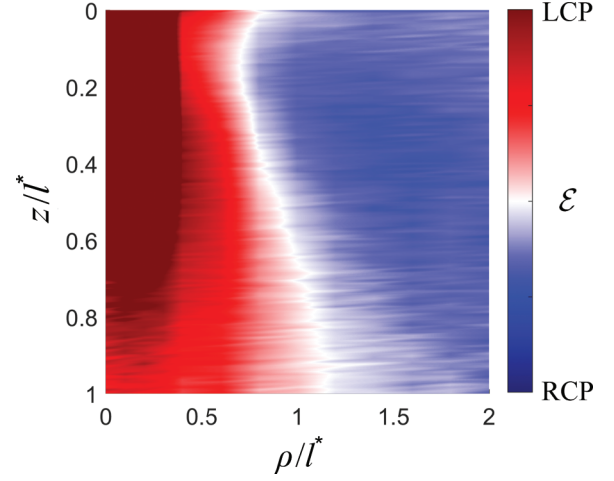

FIG. 3. In-depth spatial distribution of the polarization memory within the turbid tissuelike disordered medium in terms of PER between flipped LCP and preserved RCP components of the backscattered circularly polarized light; z/l^* is the dimensionless depth penetration and ρ/l^* is the scaled source-detector separation.

scattering angles of photons and their path-length distribution, leading to an asymmetry of the in-depth spatial distribution.

It should be pointed out that the depolarization composition of backscattered circularly polarized light varies depending on the properties of the turbid tissuelike disperse medium, such as its scattering characteristics, the size and composition of scattering particles, and the overall optical density [15–17]. From this point of view, as an example, Fig. 4 shows LCP and RCP components depending on the anisotropy of scattering (g); a deviation of the isosbestic point ($I_L = I_R$) is clearly observed.

To sum up, we focused attention on an important quantity of interest: the depolarization of circularly polarized light back-scattered from semi-infinite turbid tissuelike disperse medium. When the circularly polarized light undergoes multiple scattering events within a turbid tissuelike disordered medium, it follows a convoluted and intricate path due to interactions with the scattering particles and structures within the medium. In biological tissues these scattering particles and
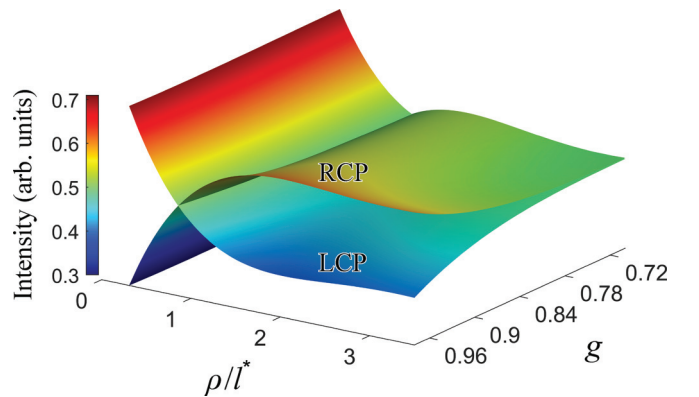

FIG. 4. LCP and RCP intensities of the backscattered light as a function of anisotropy of scattering g and source-detector separation scaled to transport length l^*.

structures include cellular components, extracellular matrices, organelles, and other microstructures. It is generally assumed that light multiply scattered from turbid tissue-like disordered medium randomizes the state of initial polarization. Multiple scattering events cause a loss of coherence of incident light. Therefore, phase relationships between different scattered waves become random, leading to the loss of initial polarization state. In other words, after undergoing multiple scattering, the polarization state of light becomes depolarized, exhibiting a mixture of polarization states. While multiple scattering tends to depolarize light, circular polarization exhibits a higher degree of preservation due to preferential scattering interactions. As a result, despite of multiple scattering the polarization memory of circularly polarized light is observed over a depolarization framework. We explore the evolution of polarization memory of circularly polarized light back-scattered from turbid tissue-like disordered medium utilizing Stokes vector formalism. More specifically, we address the in-depth binding of circular polarization memory with the helicity flips occurring within the medium. We show that for normal incidence and detection of circularly polarized light the flipped helicity survival is prevailed at the short source-detector separation ($\rho < l^*$). A transition from LCP to RCP is revealed for longer distances ($\rho > l^*$), resultant preservation of the helicity of incident light. We show that back-scattered circularly polarized light is decomposed into two fully polarized components with opposite helicities, and their polarization states are fully defined. Thus, the depolarization composition of the backscattered circularly polarized light refers to the fully polarized components of opposite helicity, their superposition resulting in some linear polarization, with no contribution from unpolarized light.

[1] D. Goldstein, *Polarized Light* (Dekker, New York, 2003).

[2] T. Novikova, I. Meglinski, J. C. Ramella-Roman, and V. Tuchin, Polarized light for biomedical applications, J. Biomed. Opt. **21**, 071001 (2016).

[3] I. Meglinski, T. Novikova, and K. Dholakia, Polarization and orbital angular momentum of light in biomedical applications: Feature issue introduction, Biomed. Opt. Express **12**, 6255 (2021).

[4] H. Chao, H. He, J. Chang, B. Chen, H. Ma, and M. J. Booth, Polarisation optics for biomedical and clinical applications: a review, Light: Sci. Appl. **10**, 194 (2021).

[5] R. P. Cameron, J. B. Götte, S. M. Barnett, and A. M. Yao, Chirality and the angular momentum of light, Philos. Trans. R. Soc. A **375**, 20150433 (2017).

[6] B. Kunnen, C. Macdonald, A. Doronin, S. Jacques, M. Eccles, and I. Meglinski, Application of circularly polarized light for non-invasive diagnosis of cancerous tissues and turbid tissue-like scattering media, J. Biophotonics **8**, 317 (2015).

[7] M. Borovkova, A. Bykov, A. Popov, A. Pierangelo, T. Novikova, J. Pahnke, and I. Meglinski, Evaluating β-amyloidosis progression in Alzheimer's disease with Mueller polarimetry, Biomed. Opt. Express **11**, 4509 (2020).

[8] M. Borovkova, O. Sieryi, I. Lopushenko, N. Kartashkina, J. Pahnke, A. Bykov, and I. Meglinski, Screening of Alzheimer's disease with multiwavelength Stokes polarimetry in a mouse model, IEEE Trans. Med. Imaging **41**, 977 (2022).

[9] A. Ushenko, A. Sdobnov, A. Syvokorovskaya, A. Dubolazov, M. Gritsuk, Y. Ushenko, A. Bykov, and I. Meglinski, Stokes-correlometry analysis of biological tissues with polycrystalline structure, IEEE J. Sel. Top. Quantum Electron. **25**, 7101612 (2019).

[10] O. Sieryi, Y. Ushenko, V. Ushenko, O. Dubolazov, A. V. Syvokorovskaya, O. Vanchulyak, A. G. Ushenko, M. Gorsky, Y. Tomka, A. Bykov, W. Yan, and I. Meglinski, Optical anisotropy composition of benign and malignant prostate tissues revealed by Mueller-matrix imaging, Biomed. Opt. Express **13**, 6019 (2022).

[11] M. Singh and I. Vitkin, Spatial helicity response metric to quantify particle size and turbidity of heterogeneous media through circular polarization imaging, Sci. Rep. **13**, 2231 (2023).

[12] F. C. MacKintosh, J. X. Zhu, D. J. Pine, and D. A. Weitz, Polarization memory of multiply scattered light, Phys. Rev. B **40**, 9342 (1989).

[13] M. Xu and R. R. Alfano, Circular polarization memory of light, Phys. Rev. E **72**, 065601(R) (2005).

[14] C. M. Macdonald, S. L. Jacques, and I. V. Meglinski, Circular polarization memory in polydisperse scattering media, Phys. Rev. E **91**, 033204 (2015).

[15] D. Bicout, C. Brosseau, A. S. Martinez, and J. M. Schmitt, Depolarization of multiply scattered waves by spherical diffusers: Influence of the size parameter, Phys. Rev. E **49**, 1767 (1994).

[16] A. H. Hielscher, J. R. Mourant, and I. J. Bigio, Influence of particle size and concentration on the diffuse backscattering of polarized light from tissue phantoms and biological cell suspensions, Appl. Opt. **36**, 125 (1997).

[17] L. F. Rojas-Ochoa, D. Lacoste, R. Lenke, P. Schurtenberger, and F. Scheffold, Depolarization of backscattered linearly polarized light, J. Opt. Soc. Am. A **21**, 1799 (2004).

[18] M. Born and E. Wolf, *Principles of Optics* (Cambridge University Press, Cambridge, UK, 2019).

[19] C. Bustamante, M. F. Maestre, and I. Tinoco, Jr., Circular intensity differential scattering of light by helical structures. I. Theory, J. Chem. Phys. **73**, 4273 (1980).

[20] *Compact Polarimeter PAX1000 Operation Manual* (Thorlabs GmbH, Bergkirchen, Ger., 2022).

[21] C. Macdonald and I. Meglinski, Backscattering of circular polarized light from a disperse random medium influenced by optical clearing, Laser Phys. Lett. **8**, 324 (2011).

[22] D. Ivanov, V. Dremin, A. Bykov, E. Borisova, T. Genova, A. Popov, R. Ossikovski, T. Novikova, and I. Meglinski, Colon cancer detection via Poincaré sphere representation and 2D polarimetric mapping of *ex vivo* tissue samples, J. Biophotonics **13**, e202000082 (2020).

[23] O. Sieryi, A. Popov, V. Kalchenko, A. Bykov, and I. Meglinski, Tissue-mimicking phantoms for biomedical applications, Proc. SPIE **11363**, 1136312 (2020).

[24] J. Chue-Sang, M. Gonzalez, A. Pierre, M. Laughrey, I. Saytashev, T. Novikova, and J. C. Ramella-Roman, Optical phantoms for biomedical polarimetry: A review, J. Biomed. Opt. **24**, 030901 (2019).

[25] A. Ishimaru, *Wave Propagation and Scattering in Random Media* (Academic, New York, 1978).

[26] I. V. Meglinski, V. L. Kuzmin, D. Y. Churmakov, and D. A. Greenhalgh, Monte Carlo simulation of coherent effects in multiple scattering, Proc. R. Soc. A **461**, 43 (2005).

[27] V. Kuzmin and I. Meglinski, Coherent effects of multiple scattering for scalar and electromagnetic fields: Monte–Carlo simulation and Milne-like solutions, Opt. Commun. **273**, 307 (2007).

[28] A. Doronin, A. Radosevich, V. Backman, and I. Meglinski, Two electric field Monte Carlo models of coherent backscattering of polarized light, J. Opt. Soc. Am. A **31**, 2394 (2014).

[29] A. Doicu and M. I. Mishchenko, An overview of methods for deriving the radiative transfer theory from the Maxwell equations. II: Approach based on the Dyson and Bethe–Salpeter equations, J. Quant. Spectrosc. Radiat. Transfer **224**, 25 (2019).

[30] A. D. Kim and M. Moscoso, Influence of the relative refractive index on the depolarization of multiply scattered waves, Phys. Rev. E **64**, 026612 (2001).

[31] T. A. Seliga, K. Aydin, and V. N. Bringi, Differential reflectivity and circular depolarization ratio radar signals and related drop oscillation and propagation effects in rainfall, Radio Sci. **19**, 81 (1984).

[32] R. M. Azzam and N. M. Bashara, *Ellipsometry and Polarized Light* (Elsevier, Amsterdam, 1989).

[33] S. R. Arridge, Photon-measurement density functions. Part I: Analytical forms, Appl. Opt. **34**, 7395 (1995).